Boundary-Layer Meteorol (2008) 129:249–268
DOI 10.1007/s10546-008-9313-y

ORIGINAL PAPER

Large-Eddy Simulation of Flow and Pollutant Dispersion in High-Aspect-Ratio Urban Street Canyons with Wall Model

Xian-Xiang Li · Chun-Ho Liu · Dennis Y. C. Leung

Received: 24 December 2007 / Accepted: 26 August 2008 / Published online: 20 September 2008

Abstract A large-eddy simulation (LES) with a one-equation subgrid-scale (SGS) model was developed to investigate the flow field and pollutant dispersion inside street canyons of high aspect ratio (AR). A 1/7th power-law wall model was implemented near rigid walls to mitigate the demanding near-wall resolution requirements in LES. This LES model had been extensively validated against experimental results for street canyons of AR = 1 and 2 before it was applied to the cases of AR = 3 and 5. A ground-level passive pollutant line source, located in the middle of the street, was used to simulate vehicular emissions. Three and five vertically aligned primary recirculations were developed in the street canyons of AR 3 and 5, respectively. The ground-level mean wind speed was less than 0.5% of the free stream value, which makes it difficult for the pollutant to be transported upward for removal. High pollutant concentration and variance were found near the buildings where the air flow is upwards. It was found that the velocity fluctuation, pollutant concentration and variance were all closely related to the interactions between the primary recirculations and/or the free surface layer. Several quantities, which are non-linear functions of AR, were introduced to quantify the air quality in street canyons of different configurations.

Keywords Large-eddy simulation (LES) · Pollutant dispersion · One-equation SGS model · Subgrid-scale (SGS) model · Wall model

1 Introduction

A "street canyon" is a relatively narrow street in between buildings that line up continuously along both sides. It constitutes the basic geometric unit of urban areas and exhibits a distinct climate where microscale meteorological processes dominate (Oke 1988). Moreover, the ventilation and pollutant removal of a street canyon occur only through its roof level.

X.-X. Li · C.-H. Liu · D. Y. C. Leung (✉)
Department of Mechanical Engineering, The University of Hong Kong, Pokfulam Road, Hong Kong, China
e-mail: ycleung@hku.hk

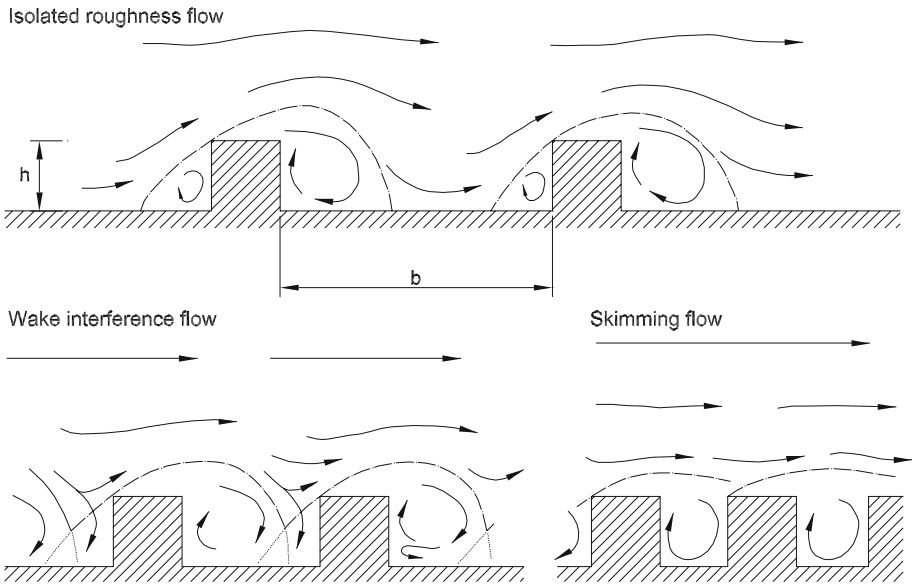

Fig. 1 Three flow regimes associated with different building-height-to-street-width ratios h/b (after Oke 1988)

Poor air quality is often observed at the pedestrian level inside these street canyons since the surrounding high-rise buildings block the approaching air flow, which in turn causes recirculations of air inside the street canyons (DePaul and Sheih 1986; Nakamura and Oke 1988).

The flow field inside a street canyon is mainly determined by the aspect ratio (AR) defined as the building-height-to-street-width ratio (h/b, where h is the building height and b the street width). The flow inside street canyons can be classified into different flow regimes depending on the AR (Fig. 1), i.e. isolated roughness flow (IRF), wake interference flow (WIF) and skimming flow (SF) regimes (Oke 1988). The dispersion behaviour of a passive and inert pollutant is closely linked to the flow pattern inside street canyons, and many studies, using field measurements, laboratory experiments, and computational fluid dynamics (CFD), have been made over the past two decades to investigate the characteristics of flow and pollutant dispersion in urban street canyons. Especially with the development of computer capacity and sophisticated numerical models, CFD has become a useful tool to explore the detailed processes that occur in street canyons and to explain the pollutant removal mechanism. Li et al. (2006) extensively reviewed the recent progress in CFD modelling of flow and air pollutant dispersion in urban street canyons.

CFD modelling in the early years mainly utilized the two-equation $k-\varepsilon$ turbulence model to account for the turbulent flow field and pollutant dispersion in street canyons. For a street canyon of low AR (AR $<$ 1), a primary recirculation was identified (Lee and Park 1994; Johnson and Hunter 1995; Baik and Kim 1999; Huang et al. 2000; Li et al. 2005), while for street canyons of higher AR (1.5 $<$ AR $<$ 2.7), two counter-rotating primary recirculations were identified (Lee and Park 1994; Baik and Kim 1999; Li et al. 2005). Furthermore, three primary recirculations were found in a street canyon of AR 3.5 (Baik and Kim 1999). Some of the above-mentioned studies also investigated pollutant transport in street canyons. Lee and Park (1994) used a street-level instantaneous pollutant source to compute the time

constant for pollutant dilution, and concluded that the pollutant transport along and across streamlines was dominated by advection and diffusion, respectively. Baik and Kim (1999) utilized a continuous pollutant line source to compute the pollutant concentration budget, by which they showed that the pollutant removal from the street canyon was dominated by vertical diffusion.

Recently, large-eddy simulation (LES) has been applied to simulate turbulent pollutant transport in street canyons. The major advantages of LES are its capability of handling the unsteadiness and intermittency of the flow, as well as providing detailed information on the turbulence structure, which, however, cannot be obtained from the $k - \varepsilon$ model. Ca et al. (1995) employed a two-dimensional (2D) LES model to study the thermal properties of urban street canyons and the corresponding impacts on the flow fields. Cui et al. (2004) had developed an LES model based on the regional atmospheric modelling system (RAMS) to simulate the air flow within and above an idealized street canyon of AR = 1 at a large Reynolds number ($\approx 2 \times 10^6$). They then extended the model to consider, for the first time, the dispersion and transport of reactive pollutants within an idealized street canyon (Baker et al. 2004). Liu and Barth (2002) and Liu et al. (2004) adopted a three-dimensional (3D) LES with a dynamic subgrid-scale (SGS) model to investigate the flow field, pollutant transport, and pollutant removal mechanism in street canyons of AR = 0.5, 1.0, and 2.0 at a Reynolds number of 12,000. Their analysis revealed that the pollutant removal was governed mainly by the roof-level turbulent diffusion on the leeward side. These findings signify that there is no mean vertical flow at the roof level. Hence LES is more reliable for the calculation of the ventilation and pollutant dispersion behaviour compared with the conventional pseudo-steady state $k - \varepsilon$ turbulence model. Based on the LES databases accumulated by Liu and Barth (2002) and Liu et al. (2004), Liu et al. (2005) examined the pollutant distribution, retention time, air exchange rate (ACH, representing the air ventilation capability of the street canyon), and pollutant exchange rate (PCH, representing the pollutant dilution capability of the street canyon). Although these LES studies have been successful in situations of low AR and Reynolds number, they are difficult to extend to street canyons of realistically high AR due to the demanding spatial resolution requirement of the dynamic model in the near-wall region.

Practically, the case of high-rise buildings surrounding a narrow street is not rare in crowded cities like Hong Kong and New York, and is very common in some Mediterranean cities like Athens (Santamouris et al. 1999). To extend the previous LES studies to high-AR street canyon problems, an LES with a one-equation SGS model has been developed and validated with an open channel flow (Li et al. 2008a, manuscript to be submitted). Usually, wall-layer models (Piomelli and Balaras 2002) are adopted in the LES technique to mitigate the demanding near-wall resolution requirement. In this study, an LES with a wall model is developed for studying the flow and pollutant dispersion inside high-AR street canyons and validated against measurements. It is then applied to simulate street canyons of AR = 3 and 5 and to investigate the characteristics of the flow field and pollutant dispersion.

2 Mathematical Model and Numerical Method

Incompressible turbulence under isothermal conditions was considered in this study, with the governing equations consisting of the Navier-Stokes equations and the continuity equation. The LES technique was used to calculate the resolved-scale motions by solving the filtered governing equations directly, and only the SGS motions were modelled. In LES, a spatial filtering is applied either explicitly or implicitly to the turbulent flow field. Based

on this filtering operation, a variable ϕ is decomposed into its resolved-scale component $\overline{\phi}$ and SGS component ϕ'. The large energy-containing resolved-scale component $\overline{\phi}$ is defined mathematically as

$$\overline{\phi}(x_i, t) = \int_{\Omega} \phi(x_i, t) G(x_i - \xi_i, \overline{\Delta})\, \mathrm{d}\xi_i, \tag{1}$$

where G is the filter function, x_i and ξ_i are the spatial coordinates in the i direction, $\overline{\Delta}$ is the filter width, and Ω is the spatial domain. This filtering process involves both flow and scalar fields, which are discussed in detail below.

2.1 Flow Equations

Applying the spatial filtering operation Eq. 1 to the governing equations yields the dimensionless resolved-scale dynamic equations

$$\frac{\partial \overline{u}_i}{\partial t} + \frac{\partial}{\partial x_j}\overline{u}_i\overline{u}_j = -\frac{\partial \overline{p}}{\partial x_i} - \frac{\partial \tau_{ij}}{\partial x_j} + \frac{1}{\mathrm{Re}}\frac{\partial^2 \overline{u}_i}{\partial x_j \partial x_j}, \tag{2}$$

and

$$\frac{\partial \overline{u}_i}{\partial x_i} = 0, \tag{3}$$

where $\overline{u}_i$ and $\overline{u}_j$ are the resolved-scale velocities in the i and j directions and $\overline{p}$ is the resolved-scale kinematic pressure. Equations 2 and 3 are expressed in tensor notation so that the indices i and j range over the spatial dimension. The reference length scale H (the building height of the street canyon of AR = 1) and the reference velocity scale U (free stream velocity) are employed to make the above equations dimensionless. The Reynolds number is defined as $Re = UH/\nu$, where ν is the kinematic viscosity. The SGS stresses

$$\tau_{ij} = \overline{u_i u_j} - \overline{u}_i\overline{u}_j \tag{4}$$

represent fluid motions at scales smaller than the filter width, and so cannot be calculated explicitly and thus need to be parametrised using a SGS model. In this study, the SGS model employed is the one-equation model (Moeng 1984; Sullivan et al. 1994), which solves an additional transport equation for the SGS turbulent kinetic energy k_{sgs} $(= \overline{u_i' u_i'}/2)$

$$\frac{\partial k_{sgs}}{\partial t} + \overline{u}_i \frac{\partial k_{sgs}}{\partial x_i} = P - \varepsilon + \frac{\partial}{\partial x_i}\left(\frac{2}{\mathrm{Re_T}}\frac{\partial k_{sgs}}{\partial x_i}\right), \tag{5}$$

where

$$P = 2\nu_{\mathrm{T}}\overline{S}_{ij}\overline{S}_{ij}, \tag{6a}$$

$$\varepsilon = C_\varepsilon \frac{k_{sgs}^{3/2}}{\ell}, \tag{6b}$$

$$\overline{S}_{ij} = \frac{1}{2}\left(\frac{\partial \overline{u}_i}{\partial x_j} + \frac{\partial \overline{u}_j}{\partial x_i}\right), \tag{6c}$$

and $\mathrm{Re_T} = UH/\nu_{\mathrm{T}}$, $\nu_{\mathrm{T}} = C_k k_{sgs}^{1/2}\ell$, with the length scale

$$\ell = \Delta = (\Delta x \Delta y \Delta z)^{1/3} \tag{7}$$

under neutral stratification (Saiki et al. 2000); C_k and C_ε are model constants. Li et al. (2008a, manuscript to be submitted) applied this model to an open channel flow and suggested an

optimum set of constants $C_k = 0.03$ and $C_\varepsilon = 1.0$. The SGS stresses are then modelled using the eddy-viscosity assumption as

$$\tau_{ij} = -2\nu_T \overline{S}_{ij}. \tag{8}$$

2.2 Wall Model

To mitigate the demanding spatial resolution requirement of LES in the near-wall regions, yet maintain a realistic description of the effect of near-wall processes on the outer flow, a wall model (wall function) is usually adopted. Based on the performance evaluation of different wall models in a periodic channel flow by Temmerman et al. (2003), the 1/7th power law (Werner and Wengle 1991) is selected to model the flow near the solid boundaries (i.e. ground, walls, and roofs). This wall model is a two-layer approximation that is based on the assumption of a 1/7th power law outside the viscous sublayer, interfaced with the linear profile in the viscous sublayer:

$$u_1^+ = \begin{cases} y_1^+ & \text{if } y_1^+ \le 11.8 \\ 8.3(y_1^+)^{1/7} & \text{if } y_1^+ > 11.8 \end{cases} \tag{9}$$

with $u_1^+ = u_1/u_\tau$, $u_\tau = \sqrt{\tau_w/\rho}$ and $y_1^+ = y_1 u_\tau/\nu$. Here, u_1 is the resolved-scale velocity tangential to the wall at the point right next to the wall in the wall-normal direction, y_1 is the distance of this point from the wall, and τ_w is the wall shear stress.

2.3 Scalar Transport Equation

Applying the filter to the passive scalar transport equation yields the dimensionless resolved-scale scalar transport equation

$$\frac{\partial \overline{c}}{\partial t} + \frac{\partial}{\partial x_i}\overline{u}_i\overline{c} = -\frac{\partial \sigma_i}{\partial x_i} + \frac{1}{\mathrm{ReSc}}\frac{\partial^2 \overline{c}}{\partial x_i \partial x_i}, \tag{10}$$

where $\overline{c}$ is the resolved-scale scalar (pollutant) mixing ratio, $\mathrm{Sc} = \nu/D$ is the Schmidt number, and D is the mass diffusivity. The first term on the right-hand side of Eq. 10 represents SGS turbulent diffusion whose fluxes

$$\sigma_i = \overline{u_i c} - \overline{u}_i\overline{c} \tag{11}$$

are smaller than the filter width and are modelled by the eddy-diffusivity model

$$\sigma_i = -\nu_c \frac{\partial \overline{c}}{\partial x_i}, \tag{12}$$

where $\nu_c = \left(1 + \frac{2\ell}{\Delta}\right)\nu_T = 3\nu_T$ (Moeng 1984; Sullivan et al. 1994; Saiki et al. 2000) according to Eq. 7.

2.4 Numerical Method

The resolved-scale dynamic equations of the mathematical model are solved by the Galerkin finite element method (GFEM) with trilinear (brick) elements to approximate the resolved-scale velocity, pressure, and scalar mixing ratio. The implicit coupling between velocity and pressure in Eqs. 2 and 3 is decoupled by the second-order accurate fractional-step method, and advection and diffusion terms in the dynamic equations are integrated in time by the

Runge-Kutta and Crank-Nicolson schemes, respectively (Ferziger and Perić 2002), both of which are second-order accurate. The non-overlapping domain decomposition technique and MPI (Gropp and Lusk 1994) are employed to achieve parallelism. The detailed numerical methodology is discussed elsewhere (Liu and Leung 2006).

2.5 Computational Domain and Boundary Conditions

Figure 2 depicts schematically the computational domain used in the current study, which represents a typical street canyon in an idealized manner. The spanwise-homogeneous computational domain consists of a street canyon of height h at the bottom and a free surface layer of height h above the buildings. The spanwise extent of the computational domain in the spanwise direction is L. This geometrical configuration represents an idealized street canyon of width b between the leeward and windward buildings of equal height h, while the free surface layer extends b_u and b_d in length in the upstream and downstream directions, respectively.

The background atmospheric flow is simulated in the form of a pressure-driven free stream in the free surface layer only. No large-scale pressure force is prescribed inside the canyon. To investigate the worst scenario of street-canyon air pollution, the approaching flow is set to be perpendicular to the street axis, which results in a free-stream wind speed U in the streamwise direction. The air flow boundary conditions are set to be periodic in the streamwise direction for the free surface layer and in the spanwise direction for the whole domain. This flow configuration represents infinitely long street canyons in the spanwise direction that are repeated infinitely in the streamwise direction. This configuration is the worst scenario of pollutant dispersion, and of relevance to urban planning and air quality improvement.

The vehicular pollutant is simulated by a ground-level continuous pollutant line source measuring L in length, placed parallel to the street axis at a distance $x_s (= 0.5b)$ from the

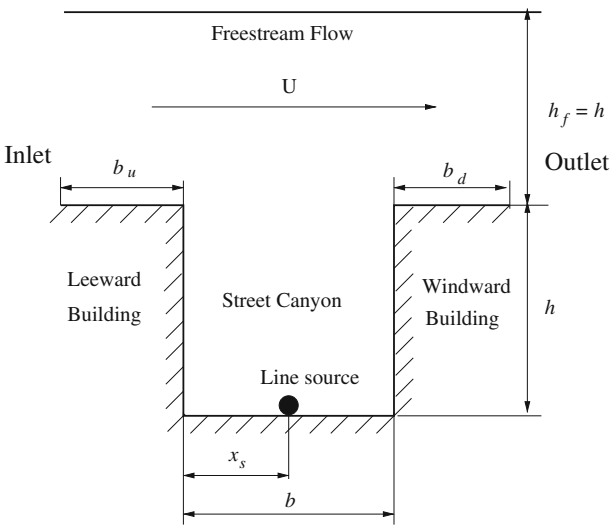

Fig. 2 Schematic diagram of the computational domain for the flow and pollutant transport in a street canyon

Table 1 Computational parameters and spatial resolution employed in the LES; H is the reference length scale, which is the building height of the street canyon of AR = 1

Aspect ratio h/b	Number of elements ($x \times y \times z$)		$\Delta x_{\min}$ or $\Delta z_{\min}$	Δy
	Street canyon	Free surface layer		
1 (coarse mesh)	$48 \times 24 \times 48$	$96 \times 24 \times 48$	$9.48 \times 10^{-3} H$	$4.17 \times 10^{-2} H$
1 (fine mesh)	$96 \times 48 \times 96$	$192 \times 48 \times 96$	$3.52 \times 10^{-3} H$	$2.08 \times 10^{-2} H$
2 (coarse mesh)	$48 \times 24 \times 96$	$96 \times 24 \times 96$	$9.37 \times 10^{-3} H$	$4.17 \times 10^{-2} H$
2 (fine mesh)	$96 \times 48 \times 192$	$192 \times 48 \times 384$	$3.52 \times 10^{-3} H$	$2.08 \times 10^{-2} H$
3 (coarse mesh)	$48 \times 24 \times 144$	$96 \times 24 \times 144$	$1.05 \times 10^{-2} H$	$4.17 \times 10^{-2} H$
5 (coarse mesh)	$48 \times 24 \times 240$	$96 \times 24 \times 240$	$9.30 \times 10^{-3} H$	$4.17 \times 10^{-2} H$

leeward building. A passive and inert pollutant is considered whose total emission rate is Q. In the free surface layer, the upstream inlet is prescribed as free of pollutants, while an open boundary condition for the pollutant

$$\frac{\partial \overline{c}}{\partial t} + \overline{u} \frac{\partial \overline{c}}{\partial x} = 0 \tag{13}$$

is used at the downstream outlet. Equation 13 allows the pollutant to pass through the downstream outlet without obvious distortion. The von Neumann (zero normal gradient) conditions for the pollutants are set on all the solid boundaries, and a periodic boundary condition for the pollutant is applied in the spanwise direction, which is the same as its flow counterpart.

2.6 Spatial and Temporal Resolution

The spatial resolution of the LES is given in Table 1. The fine spatial resolutions for street canyons of AR = 1 and 2 are based on the grid-dependence test for a street canyon of AR = 1 discussed in Liu and Barth (2002), and the results with these fine meshes will be used for sensitivity test of the current LES model in the next section.

For the flow and turbulence to achieve pseudo-steady state, the LES was integrated for 100 dimensionless time units H/U with a time increment of $0.01 H/U$. The results were then collected for another 100 dimensionless time units for statistical analysis.

3 Model Validation

The accuracy of the current LES model is evaluated by comparing the results of street canyons of AR = 1 ($h = b = H$) and AR = 2 ($h = 2H$, $b = H$) with those obtained by previous numerical models and experiments. The Reynolds number of these cases is around 15,000, which is slightly higher than that of the previous numerical and experimental studies.

In the following discussions, brackets $\langle\rangle$ represent the spanwise and temporal averages of the flow and turbulence properties, while $''$ represents the deviation from these averages.

3.1 Flow Field

The results from a previous LES model (Liu et al. 2004) and a water-channel experiment (Li et al. 2008b) are employed here to validate the prediction capability of the current LES. In the water-channel experiment, several identical model buildings (0.10 m × 0.30 m × 0.10 m in size) were aligned in a 10 m long, 0.3 m wide and 0.5 m high laboratory flume to form urban

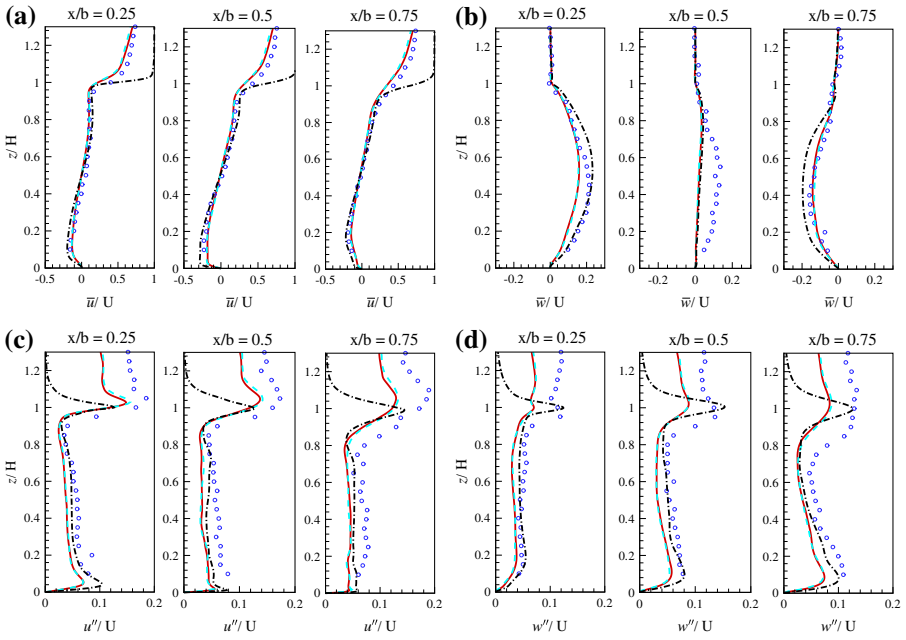

Fig. 3 Comparison of vertical profiles in the street canyon of AR = 1 by different models and experiment. ———, Calculation by the current LES model with fine mesh; – – ––, Calculation by the current LES model with coarse mesh and wall model; – · – · –, Calculation by LES (Liu et al. 2004); ○, Water-channel experiment (Li et al. 2008b)

street canyons. The water depth was about 0.40 m. The street canyons of AR = 0.5, 1.0, and 2.0 were formed by varying the distance between buildings. The velocities and fluctuating quantities were measured inside street canyons by a laser Doppler anemometer (LDA).

Figure 3 shows the comparison of vertical profiles of velocities and their fluctuations inside the street canyon of AR = 1 obtained by different numerical models and experiment, and good agreement among all the mean velocities (Fig. 3a, b) is observed inside the cavity ($z/H < 1$). It is noteworthy that, from Fig. 3b, the centre of the primary recirculation shifts downstream from the centre of the street canyon, while the numerical results indicate that the recirculation centre is very close to the canyon centre. The locations of the primary recirculation centre predicted by different numerical models and experiment are given in Table 2 for comparison. The horizontal locations predicted by most of the studies agree well with each other, although a discrepancy in the vertical location is evident, with the predictions of Jeong and Andrews (2002) much higher than others.

For the velocity fluctuations (Fig. 3c, d), the results from the numerical models and experiment generally agree well with each other, with the local maxima slightly above the roof level and with nearly constant values in the core region. Above the cavity ($z/H > 1$), the velocity fluctuations show an obvious discrepancy between different results, and is mainly due to the different configurations adopted in different numerical models and experiment. In the experiment (Li et al. 2008b), a height of $3H$ was extended above the buildings to simulate the free surface layer, while the LES by Liu et al. (2004) and the current LES used $0.5H$ and h for the free surface layer, respectively (Fig. 2). Moreover, the length of the street in the experiment is limited (about $3H$), but it is infinite in the current LES due to the periodic boundary conditions used in the spanwise direction. The end-wall effects caused by the side

Table 2 Locations of the centre of primary recirculation $(x_c/H, z_c/H)$ in street canyons of different AR being determined by numerical models and experiment

Aspect ratio	1	2	
		Upper	Lower
The current LES	(0.54, 0.53)	(0.54, 1.48)	(0.52, 0.50)
LES (Liu et al. 2004)	(0.54, 0.53)	(0.54, 1.38)	(0.53, 0.44)
$k-\varepsilon$ (Li et al. 2005)	(0.54, 0.53)	(0.55, 1.41)	(0.52, 0.37)
$k-\varepsilon$ (Jeong and Andrews 2002)	(0.56, 0.73)	(–, 1.74)	(–, 0.44)
$k-\varepsilon$ (Chan et al. 2002)	(0.54, 0.62)	–	–
$k-\varepsilon$ (Baik et al. 2000)	(0.57, 0.57)	(0.58, 1.56)	(0.54, 0.64)
Water-channel experiment (Baik et al. 2000)	(0.54, 0.58)	(0.67, 1.56)	(0.59, 0.34)

Here, x_c and z_c are, respectively, the horizontal and vertical distance measuring from the ground-level leeward corner. The reference length scale H is the building height of the street canyon of AR = 1

walls of the water channel in the experiment affect the fluctuations through the interaction between the flow in the street canyon and the boundary layer over the side walls. And because of the large eddy size in the free stream, the interaction between these large eddies and the boundary layer over the side wall is more significant than that between the small eddies inside the street canyon. Therefore the discrepancy in the free stream is larger than that inside the street canyon.

Figure 3 also shows the results of a grid sensitivity test of the current LES calculation. A fine mesh without the wall model and a coarse mesh with the wall model were applied to the same problem (Table 1). Consistent results were obtained, suggesting that the meshes adopted in the current LES model are fine enough to give grid-independent results.

Figure 4 compares the vertical profiles of velocities and their fluctuations at several locations in the street canyon of AR = 2 obtained by different numerical models and experiment. Similar to the street canyon of AR = 1, the mean velocities (Fig. 4a, b) inside the cavity ($z/H < 2$) show good agreement, while the fluctuations (Fig. 4c, d) show a relatively large discrepancy among different models. The velocity fluctuations calculated by the current LES are similar to those obtained from experiment but with a smaller magnitude. This discrepancy may partly be attributed to the end-wall effects described above, and the complicated recirculation pattern in the street canyon of AR = 2 (Li et al. 2008b).

Overall, the current LES model gives reasonably good results for velocities and fluctuations in the street canyons of AR = 1 and 2. However, there are still some discrepancies between the numerical and experimental results. Apart from the above-mentioned reasons, another possible reason may be the different averaging methods adopted in numerical calculation and experimental measurements. In the LES calculation, the flow quantities were averaged both temporally and spatially (along the spanwise direction), whereas the flow quantities were measured only at the middle vertical plane in the spanwise direction in the experiment. Besides, to simulate the urban atmospheric boundary layer, the free stream flow in the experiment was perturbed with vortex generators, making the incoming turbulence intensities higher. On the contrary, in our LES, the turbulence was generated solely by mechanical shear, whose intensities are certainly lower compared with those in the water-channel experiment. Other than these differences, the current LES employed universal values for the SGS model parameters in the whole computational domain, which might not fully account for the variation of flow properties everywhere in the domain. Some dynamic procedures have been

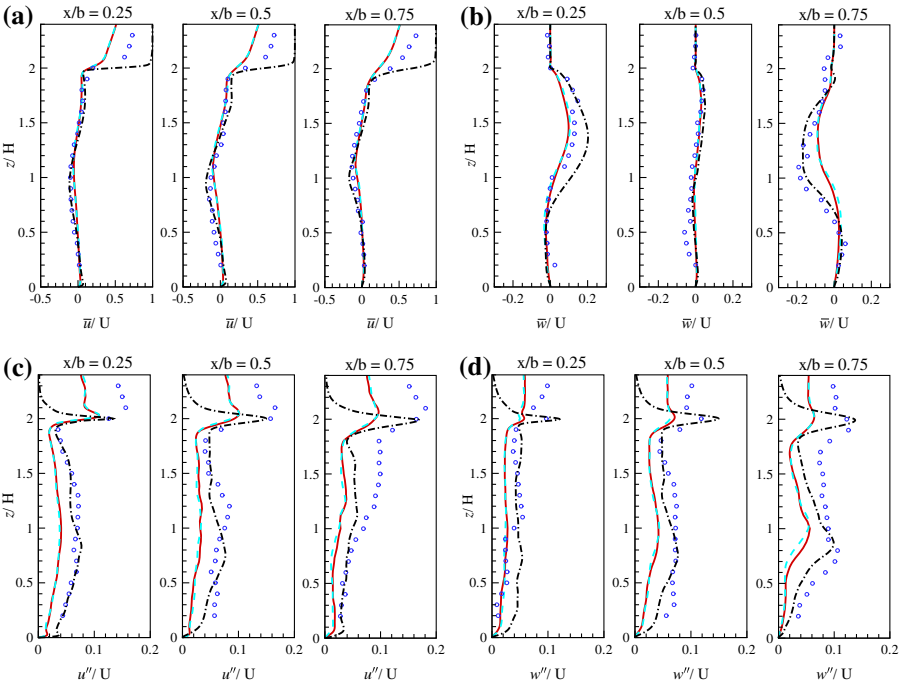

Fig. 4 Comparison of vertical profiles in the street canyon of AR = 2 by different models and experiment. Lines and symbols carry the same meanings as in Fig. 3

proposed and tested for the one-equation model (Menon and Kim 1996; Krajnović et al. 1999; Krajnović and Davidson 2001), at the expense of greatly increased computational load.

3.2 Scalar Field

Figure 5 shows the dimensionless mean pollutant mixing ratio $\langle\overline{c}\rangle UHL/Q$ along the leeward and windward walls of the street canyon of AR = 1 calculated by the current LES and data from previous wind-tunnel experiments (Pavageau 1996; Meroney et al. 1996; Pavageau and Schatzmann 1999). The current LES results with different spatial resolutions are generally consistent except at the ground-level corners, where the coarse mesh calculation with the wall model underpredicts the mean pollutant mixing ratio by 20% to 30%. The underprediction is mainly due to the two secondary recirculations near the ground-level corners (Fig. 9 in Liu and Barth 2002). Under this circumstance, the pollutants are transported to the corners mainly by turbulent diffusion. However, the coarse grid near the corners adopted in this study cannot resolve this diffusion-dominated process accurately enough. Nevertheless, the area of most concern in this study is the core region. Since the effect of the boundaries on the core region has been taken into account by means of the wall model, the details in the near-wall region are not resolved. The overall underprediction is partly caused by the coarse grid used in the LES model, and partly caused by the different configurations adopted in the calculation and the experiments, as mentioned previously. Moreover, in the experiments, the locations of measurement stations for the pollutant mixing ratio in the proximity of walls are very critical since the pollutant concentration near the walls changes sharply.

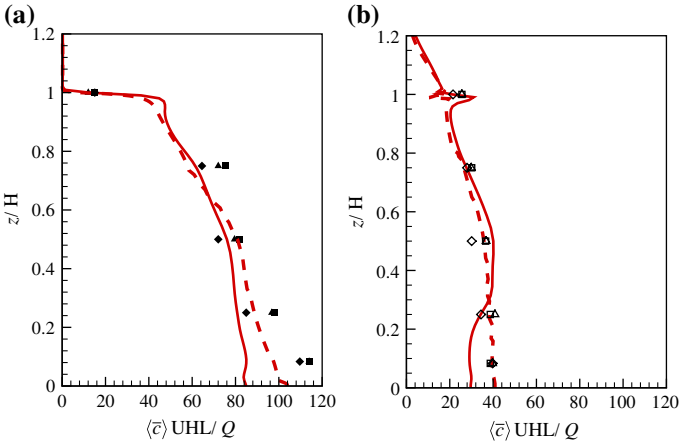

Fig. 5 Dimensionless mean pollutant mixing ratio $\langle\bar{c}\rangle UHL/Q$ on the (**a**) leeward and (**b**) windward walls of the street canyon of AR = 1. Calculated values are ———, by coarse mesh with wall model and – – ––, by fine mesh. Measured values on the windward walls are □, Pavageau (1996), ◇, Meroney et al. (1996) and △, Pavageau and Schatzmann (1999). Filled symbols represent the corresponding values on the leeward wall

The spatial distribution of the calculated dimensionless pollutant mixing ratio and its variance $\langle c''c''\rangle(UHL/Q)^2$ (with coarse mesh and wall model) is shown in Fig. 6. The calculated mean pollutant mixing ratio (Fig. 6a) agrees well with the previous wind-tunnel measurements of Pavageau and Schatzmann (1999) (Fig. 6b). However, as explained above, the current LES slightly underpredicts the pollutant mixing ratio at the ground-level leeward and windward corners due to the coarse grid used. The calculated pollutant mixing ratio variance (Fig. 6c) also agrees well with the wind-tunnel measurement at most locations. Because of the rapid mixing process in the vicinity of the line source, large gradients of both the pollutant mixing ratio and its variance are found at the ground level. A local maximum of pollutant mixing ratio variance is observed at the roof level, and the LES results suggest that this maximum is located slightly upstream. In contrast, the measurements show that it spans almost the whole width of the street. The current LES also underpredicts the magnitude of pollutant mixing ratio variance there, mainly due to the lower roof-level turbulence intensity calculated.

In conclusion, the comparison of the flow and pollutant fields between the calculation and experimental results indicates that the current LES model is capable of handling the transport processes inside street canyons and can be further applied to street canyons of higher AR.

4 Results and Discussions

After the validation, the LES with the wall model was applied to the street canyons of AR = 3 and 5 to examine the flow and pollutant dispersion features in high-aspect-ratio street canyons. For the street canyons of lower AR (0.5, 1 and 2), these features have been discussed in detail elsewhere (Liu and Barth 2002; Liu et al. 2004, 2005).

4.1 Characteristics of the Flow Field

To visualize the flow structure within the street canyons of AR = 3 and 5, the streamfunction ψ is depicted in Fig. 7, where the streamfunction ψ is defined as

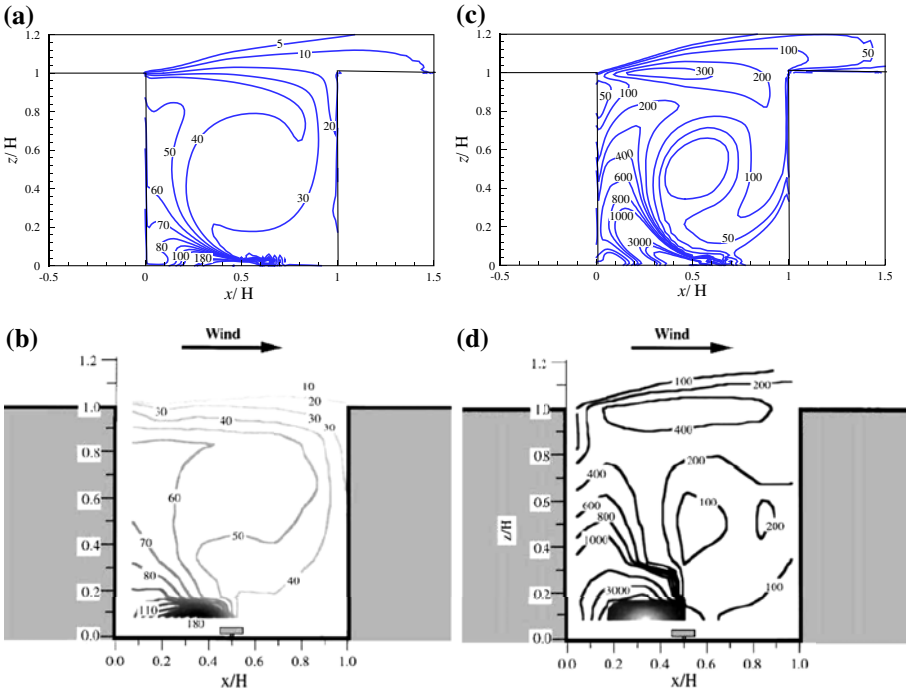

Fig. 6 Spatial distribution of dimensionless mean pollutant mixing ratio and its variance in the street canyon of AR = 1. Dimensionless mean pollutant mixing ratio $\langle \overline{c} \rangle \mathrm{UHL}/Q$ by (**a**) current LES with coarse mesh and wall model; (**b**) Pavageau and Schatzmann (1999); and dimensionless mean pollutant mixing ratio variance $\langle c'' c'' \rangle (\mathrm{UHL}/Q)^2$ by (**c**) current LES and (**d**) Pavageau and Schatzmann (1999)

$$\frac{\partial \psi}{\partial z} = \langle \overline{u} \rangle, \tag{14a}$$

$$-\frac{\partial \psi}{\partial x} = \langle \overline{w} \rangle, \tag{14b}$$

and in which a positive (negative) streamfunction indicates a counter-clockwise (clockwise) rotating recirculation. Three vertically aligned primary recirculations are formed in the street canyon of AR = 3, with the upper and lower ones rotating clockwise and the middle one rotating counter-clockwise. The roof-level air flow is similar to that of AR = 1 and 2 (Liu et al. 2004, 2005). The upper recirculation ($1.9 < z/H < 3.0$) is mainly driven by the shear of the free stream flow, and then induces another primary recirculation in the middle ($0.7 < z/H < 1.9$) through the shear, which subsequently induces the last primary recirculation at the bottom of the street canyon. Due to the reduced momentum transfer between the primary recirculations, the strength of the recirculations decreases sharply with decreasing height. The magnitude of the minimum streamfunction of the upper recirculation ($\psi = -0.03$) is about four times that of the maximum streamfunction of the middle recirculation ($\psi = 0.008$), and 30 times the magnitude of the minimum streamfunction of the lower recirculation ($\psi = -0.001$).

It is interesting to note that, in their numerical studies using a $k - \varepsilon$ model, Chan et al. (2002) and Jeong and Andrews (2002) identified two and three primary recirculations in the street canyon of AR = 3, respectively. The reason for this difference lies in the fact that the

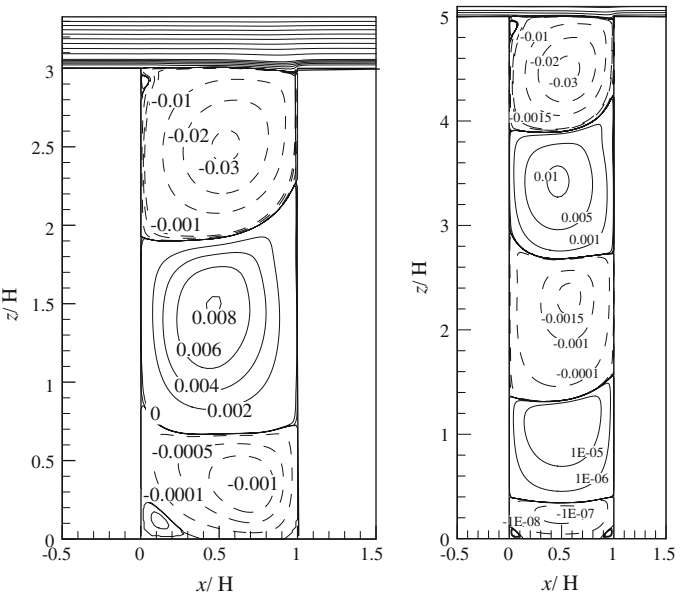

Fig. 7 Spatial distribution of the dimensionless streamfunction in the street canyon of AR (**a**) 3; (**b**) 5

current LES and the study of Jeong and Andrews (2002) investigated urban street canyons (among a group of buildings), while the street canyon studied in Chan et al. (2002) is isolated (in open country). As pointed out by Meroney et al. (1996), in the isolated case the recirculation is unstable and is discharged regularly upwards. However, in the urban street canyon, stable recirculations develop and the flow characteristics are different from those in an isolated street canyon.

In the street canyon of AR = 5, five vertically aligned primary recirculations developed (Fig. 7b), with a very weak ground-level primary recirculation. The vertical extent of the ground-level primary recirculation is only $0.5H$, half the size of the other primary recirculations. Similar to the cases of street canyons of AR = 1 and 2, three weak counter-clockwise-rotating secondary recirculations are observed at the roof-level leeward corner, and ground-level leeward and windward corners in the street canyons of AR = 3 and 5.

Figures 8a and b show the spatial variation of the normalized mean velocities $\langle\overline{u}\rangle$ and $\langle\overline{w}\rangle$, respectively, in the street canyon of AR = 3. The pattern of streamwise velocity in the street canyon can be divided vertically into four layers, separated by contour levels of zero. In the first and third layers (counting from roof level downward to ground level), the air flow is towards the windward building, while in the other two layers, the air flow is towards the leeward building. Likewise, the pattern of vertical velocity in the street canyon can be divided vertically into three layers. Within each layer, the air flows in opposite directions (upward or downward) near the opposite buildings, corresponding to the three primary recirculations depicted by the streamfunction contour (Fig. 7a). At ground level, the air moves upwards with a very small speed (around 0.5% of the free stream value), which produces little pollutant dilution near the source. The wind speed, both streamwise and vertical, decreases sharply with decreasing height in the street canyon, suppressing pollutant transport by advection, and worsening the air quality in the street canyon of AR = 3 compared with that in the street canyons of AR = 1 and 2.

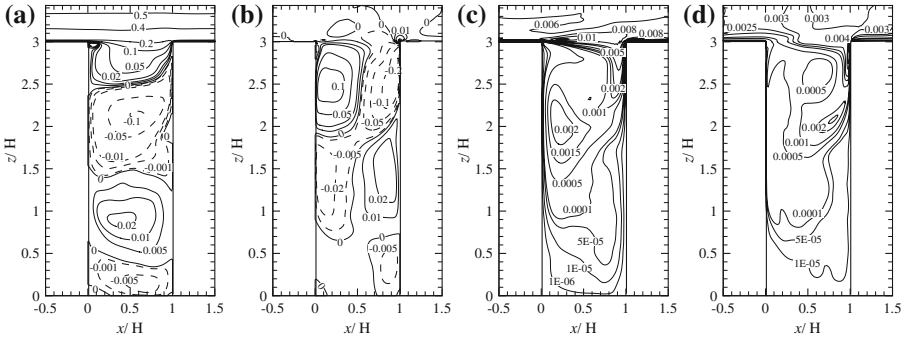

Fig. 8 Spatial distribution of dimensionless mean velocities and fluctuations in the street canyon of AR = 3 calculated by the current LES. (**a**) $\langle \overline{u} \rangle / U$; (**b**) $\langle \overline{w} \rangle / U$; (**c**) $\langle u''u'' \rangle / U^2$; (**d**) $\langle w''w'' \rangle / U^2$

To further examine the turbulence characteristics in the street canyon of AR = 3, the dimensionless velocity fluctuations $\langle u''u'' \rangle / U^2$ and $\langle w''w'' \rangle / U^2$ (Fig. 8c, d) are analyzed. The streamwise velocity fluctuation shows a local maximum of 0.01 at the roof-level leeward corner, while another local maximum of 0.002 appears near the leeward building at about $z/H = 2.0$, coinciding with the interface between the upper and middle primary recirculations. At the ground level, the magnitude of the streamwise velocity fluctuation is only 0.01% of the roof-level maximum. The vertical velocity fluctuation has a maximum of 0.004 at the roof-level windward corner, whose magnitude is only half of its streamwise counterpart. Another local maximum of 0.002 is observed near the windward building around $z/H = 2.0$, located at the same level as one of the streamwise maxima. These observations are in line with the mechanism of turbulent kinetic energy (TKE) production. At the roof level, the local maximum of velocity fluctuations is produced by the wind shear and Reynolds stress interaction between the free stream flow and the upper clockwise-rotating primary recirculation. This interaction converts the mean kinetic energy to TKE and then transfers the TKE into the street canyon following the recirculations. Other two local maxima are created by the interaction between the upper and middle primary recirculations, and their small magnitude is due to the relatively weaker wind shear compared with the free stream flow. No local maximum is found at the interface of the middle and ground-level recirculations because the ground-level recirculation is too weak, as noted above, to create any local maximum of velocity fluctuations.

Similar to the flow pattern in the street canyon of AR = 3, the spatial distribution of the streamwise and vertical velocities in the street canyon of AR = 5 (Fig. 9a, b) can also be divided into five and four layers from the roof level down to the ground level, respectively. The wind speed near the ground level is only about 0.005% of the free stream wind speed, suggesting that the pollutant dilution capability of this configuration is much worse than the case of AR = 3. This conclusion can also be drawn from the spatial distribution of velocity fluctuations shown in Fig. 9c and d. The velocity fluctuations near the ground level are several orders of magnitude less than the roof-level values, indicating that the turbulence intensity is very low there. Thus the pollutant transport at the lower street canyon will not be effective.

In general, the flow patterns in the street canyons of AR = 3 and 5 are more complex than those found in the street canyons of AR = 1 and 2. Both the velocities and turbulence intensities exhibit a feature of decreasing magnitude with decreasing height, resulting in air pollutant accumulation and air quality deterioration at the lower part of the street canyons.

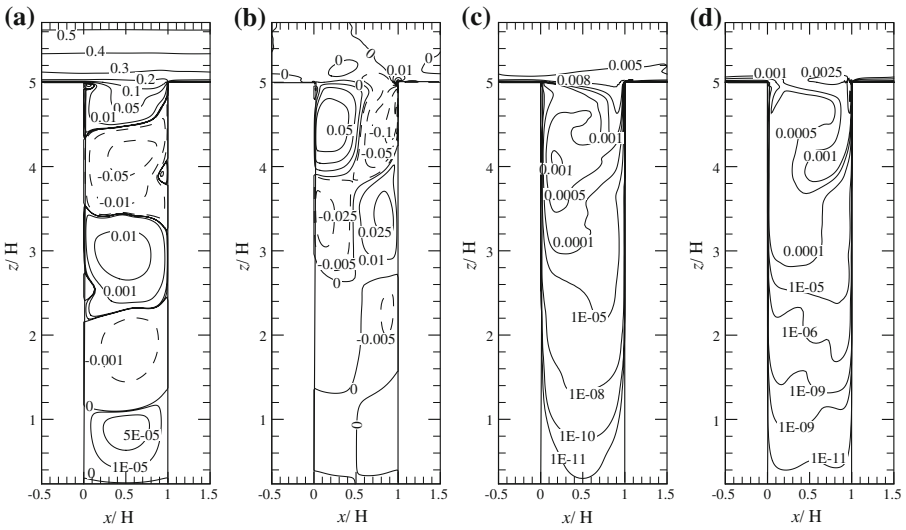

Fig. 9 Spatial distribution of dimensionless mean velocities and fluctuations in the street canyon of AR = 5 calculated by the current LES. (**a**) $\langle \overline{u} \rangle / U$; (**b**) $\langle \overline{w} \rangle / U$; (**c**) $\langle u'' u'' \rangle / U^2$; (**d**) $\langle w'' w'' \rangle / U^2$

4.2 Characteristics of Pollutant Dispersion

As described in Liu et al. (2004), pollutant movement follows the recirculation pathways in general. However, some distinct features are also observed in the pollutant dispersion inside the street canyons of AR = 3 and 5, which are discussed in this section.

The spatial distributions of mean pollutant mixing ratio and its variance in the street canyon of AR = 3 are shown in Fig. 10. Generally, the pollutant follows the primary recirculations after being emitted from the ground-level source. From roof to ground level, the spatial structure of both the pollutant mixing ratio and its variance can be divided into three layers, roughly corresponding to the three layers of the mean vertical velocities as described in the previous section. Within each layer, high pollutant concentrations and variances are generally found at locations where the air flow is upwards. This phenomenon is mainly due to the upward pollutant transport towards the roof level by advection. However, owing to the isolated nature of each primary recirculation, the upward pollutant transport is hindered by the primary recirculation or the free stream flow above it. A small portion of these upward-advected pollutants is then transported to the primary recirculation immediately above, or to the free surface layer, through turbulent diffusion. Another small portion of these pollutants is transported back by the downward air flow through advection. Eventually, a large amount of pollutants accumulates near the buildings where the air flow is upwards, leading to elevated levels of pollutant concentrations and variances.

Large pollutant concentration and variance gradients are observed not only in the wake of the pollutant line source, but also at the interfaces of primary recirculations and/or the free surface layer (Fig. 10), specifically near the three points $(x/H, z/H) = (0,\ 1.0)$, $(1.0,\ 2.25)$, and $(0,\ 3.0)$. This suggests that, when field or laboratory measurements are being performed, in addition to the wake of the line source, the rapid changes of flow and pollutant quantities at these critical points should be handled cautiously. Moreover, these large

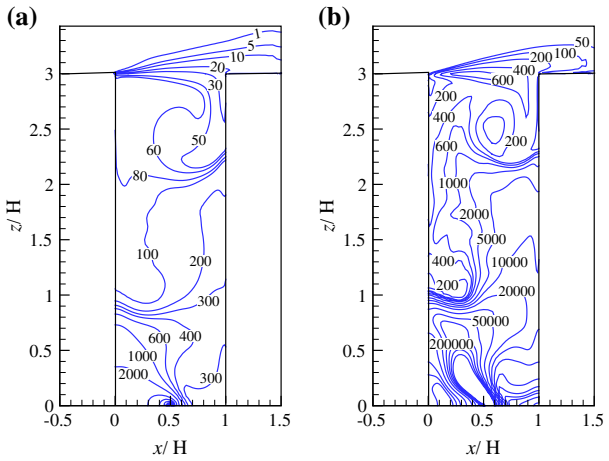

Fig. 10 Spatial distribution of dimensionless mean pollutant mixing ratio and its variance in the street canyon of AR = 3 calculated by the current LES. (**a**) scalar mixing ratio $\langle \overline{c} \rangle UHL/Q$; (**b**) scalar mixing ratio variance $\langle c'' c'' \rangle (UHL/Q)^2$

gradients manifest the intensive turbulent diffusion near those interfaces. The pollutants emitted from the line source are thus transported from one primary recirculation to another, by means of advection and turbulent diffusion, until removed from the street canyon. As a result, the efficiency of the pollutant removal depends mainly on two factors: one is the local wind speed, especially the vertical wind speed, which is responsible for carrying the pollutants toward the roof level through advection; the other is the intensity of turbulent diffusion, which is responsible for pollutant transport between primary recirculations and/or the free surface layer. In the street canyon of AR = 3, the ground-level vertical velocity is very small (Fig. 8b). Thus, the advection is very weak and the ground-level pollutant mixing ratio is at least an order of magnitude greater than at other locations within the street canyon.

Shown in Fig. 11 is the spatial distribution of mean pollutant mixing ratio and its variance in the street canyon of AR = 5. The characteristic of pollutant mixing ratio in the upper street canyon ($z/H \geq 2$) is similar to that in the street canyon of AR = 3. In contrast, in the lower part ($z/H < 2$) the pollutant mixing ratio is symmetrically distributed and decays away from the pollutant source (Fig. 11a). This phenomenon is caused by, as noted in the previous section, the dominance of molecular diffusion over advection and turbulent diffusion. On the other hand, the high accumulation of pollutants in the lower part contributes to the higher pollutant mixing ratio in the upper street canyon compared with that in the street canyon of AR = 3. Without loss of generality, one can further extrapolate that when AR further increases, the roof-level pollutant distribution is similar to that in the street canyon of AR = 3, while the ground-level distribution is similar to that in the street canyon of AR = 5.

While the coherence between the mean pollutant mixing ratios and the flow velocities is obvious (Fig. 8a,b and Fig. 10a), the coherence between the local rooftop maximum of pollutant mixing ratio variances and velocity fluctuations is also easy to identify (Fig. 8c,d and Fig. 10b). The same is true in the case of AR = 5. However, the patterns of mixing ratio variances and velocity fluctuations inside the street canyons more or less lack such coherence. This is increasingly obvious down from the roof level to the ground level, which may be due to the diminishing dominance of the flow field in the pollutant distribution, as observed above.

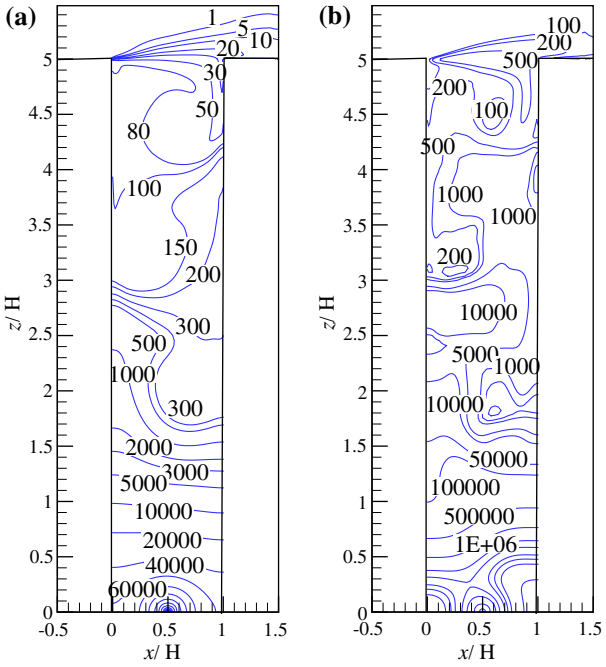

Fig. 11 Spatial distribution of dimensionless mean pollutant mixing ratio and its variance in the street canyon of AR = 5 calculated by the current LES. (**a**) scalar mixing ratio $\langle \overline{c} \rangle UHL/Q$; (**b**) scalar mixing ratio variance $\langle c'' c'' \rangle (UHL/Q)^2$

4.3 Pollutant Removal from Street Canyons

To further quantify the pollutant transport characteristics of street canyons of various ARs, several quantities based on the numerical results are introduced in this section. Making use of these quantities, one can compare the pollutant removal efficiency of different street canyon configurations.

Integrating the mean pollutant concentration $\langle \overline{c}(x_i) \rangle$ in the spatial domain

$$\langle q \rangle|_\Omega = \int_\Omega \langle \overline{c}\,(x_i) \rangle \, \mathrm{d}\Omega \,, \tag{15}$$

where Ω is the spatial domain of the street canyon or the free surface layer, yields the pollutant mass in the street canyon. The relative amounts of pollutants $\langle q \rangle$ inside the street canyons and in the free surface layer are tabulated in Table 3, where it is shown that the portions of pollutants residing in the street canyons increase with increasing AR, but the increment of portions of pollutants decreases with increasing AR, which indicates a non-linear relation between the two quantities. It is noteworthy that the portion of pollutants inside the street canyon of AR = 5 is very close to 1. For improved air quality in urban areas, this AR value may be taken as the upper bound of street configuration.

The volumetric average of Eq. 15 denotes the average pollutant concentration $\langle \theta \rangle$ in the street canyons and in the free surface layer

$$\langle \theta \rangle|_\Omega = \frac{\langle q \rangle|_\Omega}{vol_\Omega}, \tag{16}$$

where vol_Ω is the volume of Ω (street canyon or free surface layer). Pavageau and Schatzmann (1999) determined $\langle \theta \rangle \approx 55$ for a street canyon of AR = 1 from wind-tunnel measurements,

Table 3 Dimensionless pollutant distribution $\langle q \rangle$, average pollutant concentration $\langle \theta \rangle$, and retention time of pollutant $\langle \tau \rangle$ for street canyons of different aspect ratios

Aspect ratio	Pollutant distribution $\langle q \rangle$/%		Average pollutant concentration $\langle \theta \rangle$/ (Q/UHL)		Retention time
h/b	Street canyon	Free surface layer	Street canyon	Free surface layer	$\langle \tau \rangle$/T
1	93.62	6.38	43.94	1.50	43.94
2	97.89	2.11	81.03	0.97	161.96
3	99.65	0.35	370.23	0.64	1110.68
5	99.99	0.01	8820.05	0.48	44100.26

which is close to the value calculated by the current LES ($\langle \theta \rangle = 43.9$) given the low spatial resolution adopted in the wind-tunnel experiment. The average pollutant concentrations in the street canyons (Table 3) tremendously increase with increasing AR, with the highest value (corresponding to AR = 5) 200 times greater than the lowest value (corresponding to AR = 1). This observation further suggests that the pollutant concentration in the street canyon of AR = 5 is two orders of magnitude higher than that of AR = 1. As demonstrated, this quantity can be used as a measure to compare the air quality in street canyons of different configurations.

By dividing the pollutant mass $\langle q \rangle$ in the street canyon of volume $\Omega = hbL$ by the pollutant emission rate Q, the time scale of pollutant residing in the street canyons

$$\langle \tau \rangle|_{\Omega} = \frac{\langle q \rangle|_{\Omega}}{\mathrm{Q}}, \tag{17}$$

is defined as the pollutant retention time $\langle \tau \rangle$. The relation between pollutant retention time and the AR is similar to that between the average pollutant concentration and the ARs (Table 3). The longer pollutant retention time inside the street canyons is related to the poor pollutant transport between vertically aligned primary recirculations and the calm ground-level flow, as observed in the previous sections.

From the comparison of pollutant distribution, average pollutant concentration, and pollutant retention time in the street canyons of different AR, it can be found that they are all non-linear functions of AR. With the increase of AR, more and more pollutants tend to reside inside the street canyons and fewer can be removed from the street canyons.

5 Conclusion

In this study, an LES model was developed based on a one-equation SGS model and the finite element method for incompressible flow. A 1/7th wall model was implemented in this LES near the rigid walls to mitigate the high near-wall resolution requirement. This LES model was then applied to calculate the flow field and pollutant dispersion in street canyons of aspect ratio 1 and 2, and the calculated results were validated against several laboratory experiments. The validation exercise demonstrated that the current LES model gives reliable mean velocity and velocity fluctuation results in street canyons. The calculated pollutant mixing ratio and its variance were compared favorably with previous wind-tunnel measurements, and it was shown that the current LES model is capable of handling both the flow field and pollutant transport inside street canyons.

The validated LES model was then employed to simulate the street canyon of aspect ratio 3 and 5. Three and five vertically aligned primary recirculations were found inside the street canyons of AR = 3 and 5, respectively, which showed decreasing strength with decreasing height. The ground-level mean wind speeds were less than 0.5% of the free stream speed, which makes the pollutant emitted at ground level extremely difficult to transport upward to the roof level for removal. Some local maxima of the turbulence intensities were found at the interface between the free surface layer and the upper primary recirculation, and at the interfaces between the primary recirculations.

The transport of a passive and inert pollutant emitted from a line source along the centreline of the street at the ground level was simulated, and it was found that the pollutant followed the trajectories of the primary recirculations. High pollutant concentration and variance were found near the buildings where air flow was upwards. Moreover, large gradients of pollutant concentration and variance were found at the interfaces between the primary recirculations and/or the free surface layer. These findings constitute a general principle applying to street canyons of higher AR. They can also help facilitate laboratory or field measurement of pollutant transport inside street canyons.

Several quantities based on the LES results were introduced to compare the pollutant removal capability of different street canyon configurations, and it was found that these quantities were all non-linear functions of the street canyon AR. A small increment of AR would result in a dramatic increase in these quantities.

Acknowledgements The authors wish to acknowledge the Hong Kong Research Grant Council for supporting this project under grants HKU 7196/03E and 7111/04E. The authors would like to thank the Computer Centre of The University of Hong Kong for the permission to access their high performance cluster.

References

Baik JJ, Kim JJ (1999) A numerical study of flow and pollutant dispersion characteristics in urban street canyons. J Appl Meteorol 38:1576–1589

Baik JJ, Park RE, Chun HY, Kim JJ (2000) A laboratory model of urban street-canyon flows. J Appl Meteorol 39:1592–1600

Baker J, Walker HL, Cai XM (2004) A study of the dispersion and transport of reactive pollutants in and above street canyons—a large eddy simulation. Atmos Environ 38(39):6883–6892

Ca VT, Asaeda T, Ito M, Armfield S (1995) Characteristics of wind field in a street canyon. J Wind Eng Indust Aerodyn 57(1):63–80

Chan TL, Dong G, Leung CW, Cheung CS, Hung WT (2002) Validation of a two-dimensional pollutant dispersion model in an isolated street canyon. Atmos Environ 36:861–872

Cui Z, Cai XM, Baker CJ (2004) Large eddy simulation of turbulent flow in a street canyon. Quart J Roy Meteorol Soc 599:1373–1394

DePaul F, Sheih C (1986) Measurements of wind velecities in a street canyon. Atmos Environ 20:455–459

Ferziger JH, Perić M (2002) Computational methods for fluid dynamics, 3rd edn. Springer, Berlin

Gropp W, Lusk E (1994) User's guide for mpich, a portable implementation of MPI. Technical Report ANL-96/6, Argonne National Laboratory

Huang H, Akutsu Y, Arai M, Tamura M (2000) A two-dimensional air quality model in an urban street canyon: evaluation and sensitivity analysis. Atmos Environ 34:689–698

Jeong SJ, Andrews MJ (2002) Application of the $k-\varepsilon$ turbulence model to the high Reynolds number skimming flow field of an urban street canyon. Atmos Environ 36:1137–1145

Johnson GT, Hunter LJ (1995) A numerical study of dispersion of passive scalars in city canyons. Boundary-Layer Meteorol 75:235–262

Krajnović S, Davidson L (2001) Large eddy simulation of the flow around a three-dimensional bluff body. AIAA paper 01-0432

Krajnović S, Müller D, Davidson L (1999) Comparison of two one-equation subgrid models in recirculating flows. In: Voke PR, Sandham ND, Kleiser L (eds) Direct and large-eddy simulation III. Kluwer, The Netherlands, pp 63–74

Lee IY, Park HM (1994) Parameterization of the pollutant transport and dispersion in urban street canyons. Atmos Environ 28:2343–2349
Li XX, Liu CH, Leung DYC (2005) Development of a $k-\varepsilon$ model for the determination of air exchange rates for street canyons. Atmos Environ 39(38):7285–7296
Li XX, Liu CH, Leung DYC, Lam KM (2006) Recent progress in CFD modelling of a wind field and pollutant transport in street canyons. Atmos Environ 40:5640–5658
Li XX, Liu CH, Leung DYC (2008a) Development of an FEM LES with one-equation subgrid-scale model for incompressible flow. Submitted to Comput Method Appl M Eng
Li XX, Leung DYC, Liu CH, Lam KM (2008b) Physical modeling of flow field inside urban street canyons. J Appl Meteorol Climatol 47(7):2058–2067
Liu CH, Barth MC (2002) Large-eddy simulation of flow and scalar transport in a modeled street canyon. J Appl Meteorol 41(6):660–673
Liu CH, Leung DYC (2006) Finite element solution to passive scalar transport behind line sources under neutral and unstable stratification. Int J Num Methods Fluids 50(5):623–648
Liu CH, Barth MC, Leung DYC (2004) Large-eddy simulation of flow and pollutant transport in street canyons of different building-height-to-street-width ratios. J Appl Meteorol 43:1410–1424
Liu CH, Leung DYC, Barth MC (2005) On the prediction of air and pollutant exchange rates in street canyons of different aspect ratios using large-eddy simulation. Atmos Environ 39:1567–1574
Menon S, Kim WW (1996) High Reynolds number flow simulations using the localized dynamic subgrid-scale mode. AIAA paper 96-0425
Meroney RN, Pavageau M, Rafadalis S, Schatzmann M (1996) Study of line source characteristics for 2D physical modelling of pollutant dispersion in street canyons. J Wind Eng Industr Aerodyn 62:37–56
Moeng CH (1984) A large-eddy-simulation model for the study of planetary boundary-layer turbulence. J Atmos Sci 4(13):2052–2062
Nakamura Y, Oke TR (1988) Wind, temperature, and stability conditions in an east-west-oriented urban canyon. Atmos Environ 22:2691–2700
Oke TR (1988) Street design and urban canopy layer climate. Energy Build 11:103–113
Pavageau M (1996) Concentration fluctuations in urban street canyons - groundwork for future studies. Technical report, Meteorological Institute of the University of Hamburg, 97 pp
Pavageau M, Schatzmann M (1999) Wind tunnel measurements of concentration fluctuations in an urban street canyon. Atmos Environ 33:3961–3971
Piomelli U, Balaras E (2002) Wall-layer models for large-eddy simulations. Ann Rev Fluid Mech 34:349–374
Saiki EM, Moeng CH, Sullivan PP (2000) Large-eddy simulation of the stably stratified planetary boundary layer. Boundary-Layer Meteorol 95:1–30
Santamouris M, Papanikolaou N, Koronakis I, Livada I, Asimakopoulos D (1999) Thermal and air flow characteristics in a deep pedestrian canyon under hot weather conditions. Atmos Environ 33(27):4503–4521
Sullivan PP, McWilliams JC, Moeng CH (1994) A subgrid-scale model for large-eddy simulation of planetary boundary-layer flows. Boundary-Layer Meteorol 71(3):247–276
Temmerman L, Leschziner MA, Mellen CP, Froöhlich J (2003) Investigation of wall-function approximation and subgrid-scale models in large eddy simulation of separated flow in a channel with streamwise periodic constrictions. Int J Heat Fluid Flow 24:157–180
Werner H, Wengle H (1991) Large-eddy simulation of turbulent flow over and around a cube in a plate channel. In: 8th symposium on turbulent shear flows, pp 155–168